International Journal of Bioprinting

RESEARCH ARTICLE

Commercial articulated collaborative *in situ* 3D bioprinter for skin wound healing

Aleksandr A. Levin[1†*], Pavel A. Karalkin[2,3†*], Elizaveta V. Koudan[1], Fedor S. Senatov[1], Vladislav A. Parfenov[4], Vladislav A. Lvov[1], Stanislav V. Petrov[1], Frederico D. A. S. Pereira[5], Alexey V. Kovalev[6], Egor O. Osidak[7,8], Sergey P. Domogatsky[7], Natalya E. Manturova[9], Vladimir A. Kasyanov[10], Natalia S. Sergeeva[2], Vadim L. Zorin[11,12], Yusef D. Khesuani[5], Vladimir A. Mironov[1,6]

[1]Center for Biomedical Engineering, National University of Science and Technology "MISIS", Moscow, Russia

[2]National Medical Research Radiological Center, P. A. Hertsen Moscow Oncology Research Center, Moscow, Russia

[3]L. L. Levshin Institute of Cluster Oncology, Sechenov First Moscow State Medical University, Moscow, Russia

[4]A. A. Baikov Institute of Metallurgy and Material Science, Russian Academy of Sciences, Moscow, Russia

[5]Laboratory for Biotechnological Research "3D Bioprinting Solutions", Moscow, Russia

[6]Priorov Central National Institute of Traumatology and Orthopedics, Moscow, Russia

[7]Imtek Ltd., Moscow, Russia

[8]Dmitry Rogachev National Medical Research Center of Paediatric Haematology, Oncology and Immunology, Moscow, Russia

[9]JSC Plastic Surgery and Cosmetology Institute, Moscow, Russia

[10]Joint Laboratory of Traumatology and Orthopedics, Riga Stradins University, Riga, Latvia

[11]Human Stem Cells Institute, Moscow, Russia

[12]SKINCELL LLC, Skolkovo, Moscow, Russia

[†]These authors contributed equally to this work.

***Corresponding authors:**
Aleksandr A. Levin (levin.alexandr.stankin@gmail.com)
Pavel A. Karalkin (pkaralkin@gmail.com)

Citation: Levin AA, Karalkin PA, Koudan EV, 2023, Commercial articulated collaborative *in situ* 3D bioprinter for skin wound healing. *Int J Bioprint.* 9(2): 675. https://doi.org/10.18063/ijb.v9i2.675

Received: December 1, 2022

Accepted: December 13, 2022

Published Online: January 31, 2023

Abstract

In situ bioprinting is one of the most clinically relevant techniques in the emerging bioprinting technology because it could be performed directly on the human body in the operating room and it does not require bioreactors for post-printing tissue maturation. However, commercial *in situ* bioprinters are still not available on the market. In this study, we demonstrated the benefit of the originally developed first commercial articulated collaborative *in situ* bioprinter for the treatment of full-thickness wounds in rat and porcine models. We used an articulated and collaborative robotic arm from company KUKA and developed original printhead and correspondence software enabling *in situ* bioprinting on curve and moving surfaces. The results of *in vitro* and *in vivo* experiments show that *in situ* bioprinting of bioink induces a strong hydrogel adhesion and enables printing on curved surfaces of wet tissues with a high level of fidelity. The *in situ* bioprinter was convenient to use in the operating room. Additional *in vitro* experiments (*in vitro* collagen contraction assay and *in vitro* 3D angiogenesis assay) and histological analyses demonstrated that *in situ* bioprinting improves the quality of wound healing in rat and porcine skin wounds. The absence of interference with the normal process of wound healing and

even certain improvement in the dynamics of this process strongly suggests that *in situ* bioprinting could be used as a novel therapeutic modality in wound healing.

Keywords: *In situ* bioprinting; Wound healing; Bioink; Collagen hydrogel

1. Introduction

Bioprinting is defined as a robotic layer by layer or additive biofabrication of functional tissue and organ constructs from living cells and biomaterials (usually hydrogel) according to digital model[1-6]. To perform bioprinting, it is necessary to have digital model of tissue and organ construct, bioink, or hydrogel loaded with living cells and bioprinter[7-9]. Due to its relative anatomical and histological simplicity, bioprinting of human skin became one of most popular topics in the rapidly emerging bioprinting research field[10-12]. There are two main approaches in skin bioprinting technology: (i) *In vitro* bioprinting and (ii) *in situ* bioprinting. In the first case, skin construct must be at first bioprinted in clean room or in so-called good manufacturing practice (GMP) facilities and during post-processing, bioprinted skin constructs must undergo accelerated tissue maturation in specially designed bioreactor[13-15]. In case of so-called *in situ* (or *in vivo* or intraoperational) bioprinting, biofabrication of human skin could be performed directly on the patient body in operating room and it does not require GMP facilities. Moreover, human body will serve as some sort of bioreactor, and thus, there is a need in specially designed bioreactor. Thus, *in situ* skin bioprinting has certain advantage and represent a cost-effective alternative as compared with more conventional *in vitro* skin bioprinting[16-21]. Robotic bioprinter is a key element of bioprinting system. There are already several dozen companies producing commercial *in vitro* three-dimensional (3D) bioprinters[22] and even first attempts to develop original custom made *in situ* bioprinter in academic setting[23-25] but, to the best of our knowledge, there are commercially available *in situ* bioprinter. On the other hand, there is a growing interest to develop relatively cheap and affordable *in situ* handheld printers[26-30] which, however, are inferior option because they are not robotic driven and thus do not follow specially designed digital models. The purpose of this work was to describe the design, fabrication, and initial *in vitro* and *in vivo* testing of *in situ* 3D bioprinter. To the best of our knowledge, this is the first description of commercially available commercial articulated collaborative 3D bioprinter suitable for *in situ* skin bioprinting. Pre-clinical testing on specially designed animal models of human skin diseases and sequential certification and regulatory agencies approval for clinical use will enable highly desirable clinical translation and commercialization of this technology.

2. Materials and methods

2.1. Hardware

The *in situ* printing scheme on a living organism includes a robotic arm KUKA Sunrise Cabinet (KUKA, Germany) that performs flexible programming in a high-level Java language (Figure 1). An extruder based on an electric motor for hydrogel extrusion was used, since it is more convenient to use and does not require a compressor for compressed air. In addition, the scheme uses a real-time breathing skin displacement sensor, a robot controller and a personal computer (PC) (Figure 2). In this case, the computer and the end effector are connected through USB, as well as the computer and the robot controller are connected through TCP/IP protocol.

The compact structure of the end effector consists of a cooling system, a controller of the end effector, a Fishman dispenser, and a biomaterial (Figure 3A). The compactification of the technical solution was achieved by placing the entire electrical part on the end effector in the control unit. All electrical components, such as voltage converters, a stepper motor control driver, and a control microcontroller of the end effector, were attached to the main body of the control unit. The block was closed with a lid from above (Figure 3B), which provided the protective properties of electrical components from external environmental influences. The housing and holder of the dispenser itself, which attached the end effector to the flange of the robot (Figure 3B), was made by FDM using the Ultimaker 2 3D printer (Ultimaker B.V., Netherlands). The structure also includes several programmable devices: A robot controller, an end effector, and a PC. At the same time, it is worth noting that communication and management of all devices in the system were facilitated with the help of a PC.

The choice of the dispenser is due to the fact that it has already been used in the 3D bioprinter Fabion (3D Bioprinting Solution, Russia) and has proven itself to be a convenient and reliable dispenser of biomaterials. An important advantage is the possibility of flexible controlled material supply. The stem tip has a screw thread into which the syringe piston is screwed, which allows both extrusion and suction of the material and is very important when working with viscous materials having inertia. The dispenser squeezes out the material using a stepper motor,

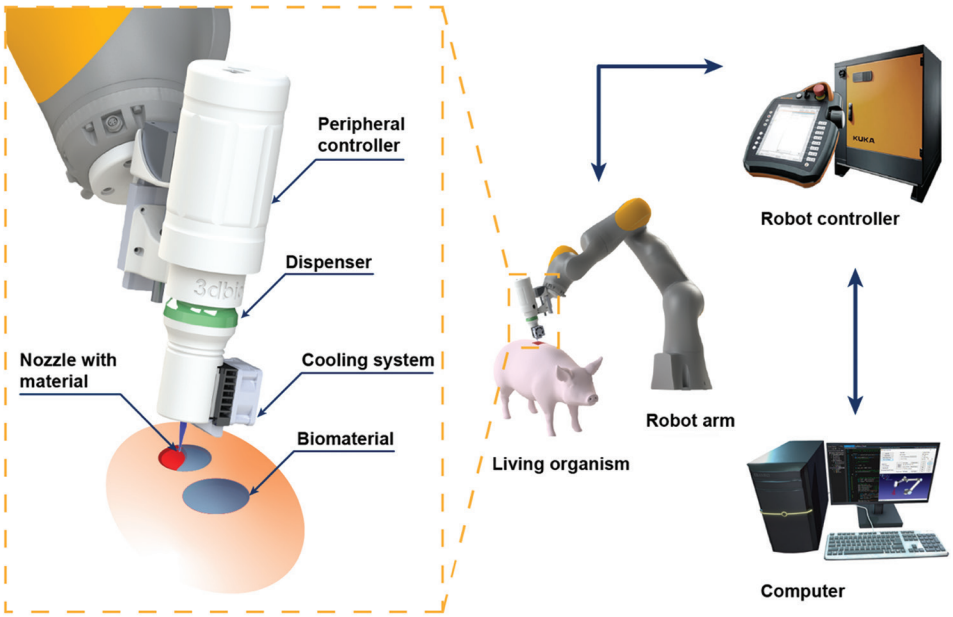

Figure 1. Scheme of *in situ* bioprinting system.

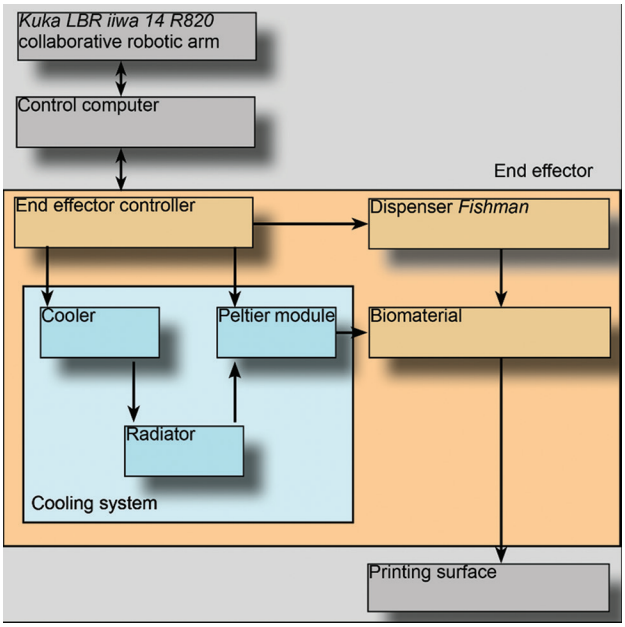

Figure 2. Design of *in situ* head.

and the TMC2100 driver (Trinamic, Germany) was used to control it. The Arduino programming platform was used as a microcontroller controlling the end effector.

2.2. Cooling system

The end effector uses a syringe cooling system based on a Peltier module, which, when voltage is applied to it, cools one side and heats the other (Figure 3). The material to be printed is polymerized (stitched) if the ambient temperature is above 10°C. Since the operating room usually has a temperature of about 20°C, it is necessary to ensure the material is cooled in the syringe. A metal part is adjacent to the cooling side, which provides cooling of the syringe. A radiator was attached to the heated side of the module for rapid heat outflow, and a cooling fan was used to improve the heat sink. All components were attached to the housing, which reduced the heat exchange of the metal part with the external environment.

2.3. Electrical diagram

The provision of digital control of the cooling system was carried out using the Cytron MD13S driver (Cytron Technologies Sdn Bhd, Malaysia), which is able to control devices with the necessary power. In the cooling system, a voltage of 6V was used for cooling, while the current consumption of the cooling system corresponds to 1 A. The LM2596S-ADJ (Semiconductor Components Industries, USA) boards were used as voltage converters in electrical coupling, which not only lowered the voltage but also stabilized it. A voltage of 9 V was used for the stepper driver and 6 V for the Peltier module. For the general power supply of the system, a DC power supply with a voltage of 12 V and a maximum current of 2 A were used.

2.4. Software

When bioprinting, it is important that the robot's movements and the volume of the material being squeezed out are consistent with each other. Special software has been developed to implement this condition. Special

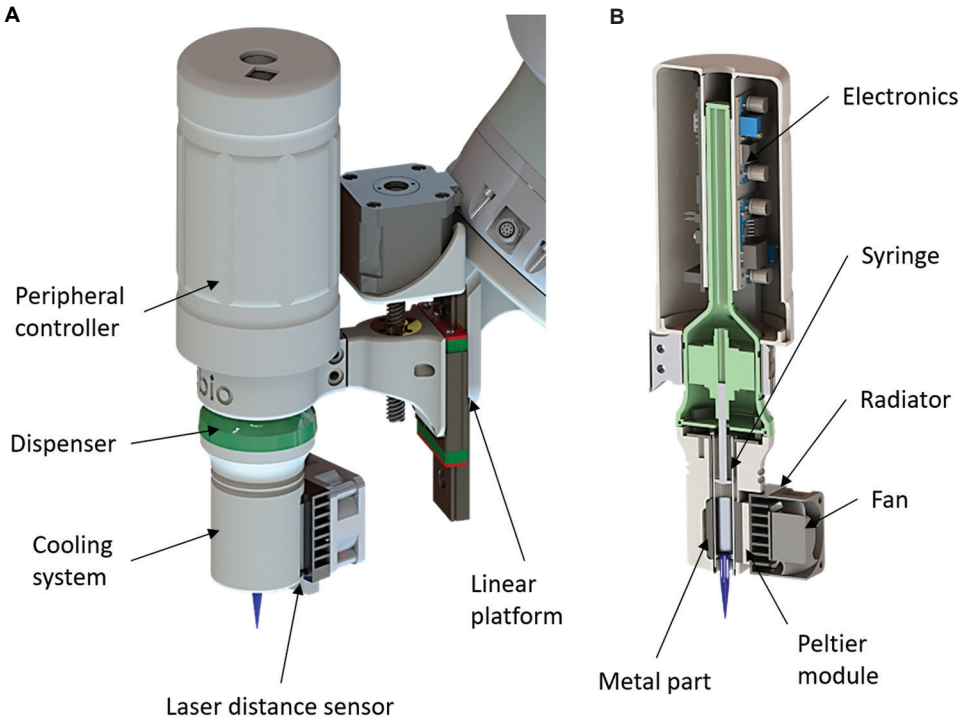

Figure 3. Structure of printhead in *in situ* bioprinting system: (A) External view and (B) sectional view.

software has been developed for the robotic bioprinter. The user interface with the ability to display a 3D representation of trajectories was written in the Python programming language using the Pyqt5 and OpenGL libraries. The trajectory generated by the program takes into account the curvature of the surface, which allows for bioprinting on surfaces of complex shape. The use of distance sensors on the end effector allows users to take into account the change in the position of the surface, which occurs due to breathing. It is worth noting that all the software is publicly available and gives interested parties the opportunity to improve it and use it for their own purposes. The developed software is focused not only on narrow specialists but also on operators with minimal training, since the program structure is designed in such a way to minimize the human factor.

2.5. The algorithm of the bioprinter system

The controller of the printing device operates according to the following algorithm. The program is in an infinite loop and is waiting for a message from the control computer, which contains information about how fast and how many steps the nozzle piston should move, and whether the cooling system should be turned on now or not. In turn, the robot controller first sends the coordinates of the points that characterize the wound surface. Then, an array of trajectory data comes from the control computer, which also includes information about the volume of the material being squeezed out. The trajectory is a set of short lines. Next, the program waits for the operator's permission to start printing. If the resolution is obtained, the robot starts moving along each line with a minimum smoothing radius, while maintaining a constant linear speed. This allows for uniform application of the material. At the same time, to ensure non-stop operation, commands are executed on the robot in asynchronous mode, that is, the internal robot controller responsible for interpolating robot movements is several commands ahead of the upper level robot controller.

The following algorithm is used to synchronize the movement of the robot and the extrusion of the material. During the execution of the trajectory, the robot sends a command to build the next line only after it passes the point of the line two commands back. To do this, the robot checks its current coordinate and compares it with the coordinate of the end of the current line.

2.6. Reagents

Dulbecco's Modified Eagle's Medium (DMEM, cat.# 12491-015), M200 medium (cat.# M200500), fetal bovine serum (FBS, cat.# 16000-044), antibiotic-antimycotic (cat.# 15240-062), trypsin/EDTA (cat.# 25200-114), and phosphate-buffered saline (PBS, cat.# 18912-014) were obtained from Gibco (USA). L-glutamine (cat.# F032),

EDTA solution (cat.# R080), and sodium hydrocarbonate (cat.# F022E) were purchased from Paneco (Russia). Sodium hydroxide (cat.# 1.06498) was obtained from Merck (Germany). DAPI (cat.# D1306) was purchased from Invitrogen (USA).

2.7. Cell culture

Human umbilical vein endothelial cells (HUVECs) was purchased from PromoCell (cat.# C-12203). Human dermal fibroblasts (HFs) were obtained from Lonza (cat.# CC-2511). HUVECs were grown in a M200 medium, supplemented with low serum growth supplement and antibiotic/antimycotic. HF cells were grown in DMEM containing 10% FBS. Primary cultures of rat and porcine fibroblasts were isolated after mechanical treatment and disaggregation of skin samples followed by incubation with 0.25% trypsin and 200 U/ml collagenase-I solution. The resulting suspension was filtered and transferred to a DMEM culture containing 10% FBS, supplemented with antibiotic/antimycotic and 2 mM L-glutamine. The cells were incubated at 37°C in a humidified atmosphere with 5% CO_2 and routinely split at 85%–95% confluence with trypsin/EDTA solution. According to DAPI staining protocol, cells were confirmed free of mycoplasma contamination.

2.8. Tissue spheroids formation

The tissue spheroids from HUVEC and 50% HUVEC + 50% HF mixture were formed using Corning spheroid microplates (Corning, cat.# 4520), according to the manufacturer's protocol. Briefly, cells in a monolayer with 95% confluence were rinsed with EDTA solution, harvested from the substrate by 0.25% trypsin/0.53 mM EDTA, and then resuspended in a cell culture medium. The cell concentration was 3×10^4/mL. Finally, 100 μL of cell suspensions were delivered into the wells of Corning spheroid microplates. Corning spheroid microplates were incubated at 37°C in a humidified atmosphere with 5% CO_2.

2.9. Collagen isolation from rat tails and collagen gel preparation

A commercial solution of "Viscoll" sterile porcine collagen[31] at a concentration of 80 mg/mL was used for *in situ* bioprinting experiments. Before bioink preparation, the collagen solution was neutralized with transparent DMEM (without phenol red) containing TRIS buffer (pH 7.2–7.4). The pooled rat and porcine platelet lysate samples were prepared as described previously[32] and the skin fibroblast cell suspension was added to prepare the complete bioink recipe. The resulted composition contained 10% platelet lysate and 1 million cells/mL of hydrogel solution.

To assess the effect of platelet lysate on gel contraction and tissue spheroid spreading, it was added to the collagen solution at a concentration of 10%. For the preparation of collagen gel, 890 μL of collagen solution was mixed with 60 μL of 1 M sodium hydroxide, 250 μL of 7.5% sodium bicarbonate, and 300 μL of PBS (for collagen gel) or 150 μL of PBS + 150 μL of platelet lysate (for collagen + platelet lysate gel).

2.10. Contraction assay

HF cells were harvested from confluent cultures using 0.25% trypsin/0.53 mM EDTA, counted, adjusted to the desired density, and resuspended in a solution of polymerizing collagen. Aliquots (100 μL) of the cell-collagen mixture were dispensed into 96-well cell culture plate. The hydrogel was subjected to polymerization at 37°C for 1 h, and then, culture medium was added. The gels were then gently detached from the walls of the plate wells by passing a medical needle around the perimeter of the gels. In 48 h, brightfield images of gels were obtained using the "SMZ18" stereomicroscope (Nikon, Japan). The sample areas were measured using ImageJ 1.48v software (NIH, Bethesda, MD). All original images were converted to simplified threshold images under the same converting condition, and the edges of the samples were manually detected. The sample areas were first measured as pixels and then converted to micrometers by comparing them to a reference length. The results of the contraction assay were expressed in percentage relative to the initial sample areas considered to be 100%.

2.11. Tissue spheroid spreading assay

The tissue spheroids were formed from 3000 cells using Corning spheroid microplates. One-day-old tissue spheroids were embedded in the collagen and loaded into 24-well plates (Corning, Cat.# 3337). The hydrogel was subjected to polymerization at 37°C for 1 h, and then, culture medium was added. In 48 h, spheroids were labeled with live/dead kit to visualize live and dead cells. Brightfield and fluorescent images of spheroids were obtained using the "Eclipse Ti-S" microscope (Nikon, Japan). The spreading areas and densities were measured using ImageJ 1.48v software (NIH, Bethesda, MD). The spreading areas were expressed in percentage relative to the initial spheroid areas considered to be 100%. The densities were calculated as a fraction of cells, spreading and forming spheroid, in comparison with total image area which was consistent for all images.

2.12. *In vivo* experiments

To perform *in situ* bioprinting experiments, 30 male Wistar rats and six male Wiesenau minipigs were used.

In vivo experiments were performed at the Veterinary Department of the National Medical Research Center for Radiology and were approved by the local ethics committee (protocol #0120/19 dated November 1, 2019). Throughout the experiment, the animals were kept in individual ventilated boxes under exhaust ventilation and were fed *ad libitum*. The animal work was carried out in accordance with the ethical principles established by the European Convention for the Protection of Vertebrate Animals used for Experimental and Other Scientific Purposes (Strasbourg, 2006) and the International Guidelines for Biomedical Research in Animals (CIOMS and ICLAS, 2012). Circular full-thickness skin defects were formed using sterile surgical instruments after preliminary intravenous Zoletil/Xylazine sedation of animals. In the case of minipigs, the isoflurane inhalation anesthesia was additionally used. Robotic-assisted bioprinting with hydrogel compositions was carried out immediately after the wound preparation and cleaning. The polymerized bioprinted collagen hydrogels in wounds were carefully covered with dressings. All animals received intramuscular antimicrobial and analgesic drugs for 1 week after surgery.

2.13. Adhesiometric analysis

Hydrogel adhesion to non-injured and injured rat skin was estimated using commercial adhesion tester (Figure 4A and B). At least five non-injured and five injured excised rat skin specimens were used. The standard micro-incisions were made with a medical scalpel to form model injuries on the skin surface. The statistical analysis of adhesiometry results was performed.

2.14. Histological and morphometrical analysis

After excision, skin tissue samples were fixed in PBS-buffered 4% paraformaldehyde solution (Sigma-Aldrich, USA) and embedded in paraffin (BioVitrum, Russia). Dewaxing was carried out using xylene and a battery of downstream alcohols. Serial sections with a thickness of 4 μm were cut with Microtome Microm HM355S (Thermo Fisher Scientific, USA), mounted on poly-L-lysine coated glasses, and routinely stained with hematoxylin-eosin dye (BioVitrum, Russia).

Morphometry histological sections were performed using automated image analysis system (ImageJ, USA) and quantitative morphometric parameters such as inflammatory index (number of inflammatory cells per unit of analyzed histological section area) and angiogenesis index (number of microvessels profile per unit of analyzed histological section area) were estimated with sequential statistical analysis.

2.15. Statistical analysis

Statistical data were analyzed and graphs were plotted using GraphPad Prism software (GraphPad Software, Inc., La Jolla, CA) and expressed in mean ± standard deviation. The Mann–Whitney U-test was used to compare the quantitative characteristics of the groups. Statistical significance was determined at $P < 0.05$.

3. Results

3.1. Feedback system

Since the patient is breathing during bioprinting, it is necessary to take into account the displacement of the surface on which the bioprinting is carried out. To do this, a feedback system was integrated into the end effector, consisting of a laser sensor next to the nozzle and a linear actuator that moves the end effector relative to the robot flange. UL53 was chosen as the sensor, which operates on the ToF (Time of flight) principle, which allows for better accuracy on surfaces presented in the form of soft tissues. The program sets the distance that the nozzle should hold to the surface, and in accordance with this, the controller sends commands to the linear driver of this system. Optimal algorithms for filtering the signal from the distance sensor were selected for performing the operation on animals.

3.2. Trajectory generation

The program on the control computer is a graphical interface with the ability to start and stop the bioprinting

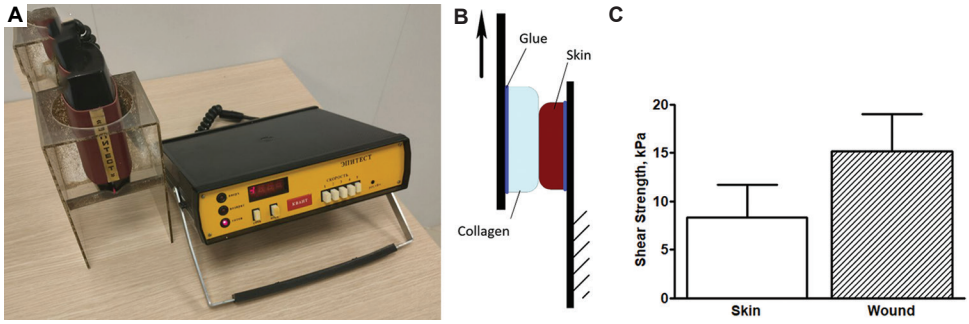

Figure 4. (A) Commercial adhesion tester. (B) Scheme of measuring the adhesion of hydrogel to the skin. (C) Measurement result of shear strength.

process. It also provides the ability to manually control the printer.

With the help of SprutCAM software, a trajectory for the plane is generated based on a 3D model of the defect. Thus, we set the main printing parameters, such as the thickness of the filament, the printing speed, and the filling method. When the user presses the command to start printing, the program sends a message to the robot controller about the start of printing, and the robot controller responds by sending points characterizing the printing surface. The program decrypts the file with the trajectory and is saved as an array, while all lines are divided into short ones with a length of 1 mm. Then, according to the loaded points, the trajectory is cut along the border. Then, the equations of the surface are calculated from the points, and the trajectory is projected onto the resulting surface. Thus, an array of lines is obtained, which is already transmitted to the robot controller. After that, the program starts working in the link mode between the robot controller and the printer controller. The program sends messages about the supply of material from the robot controller to the controller of the printing device.

3.3. *In situ* bioprinting process

The robotic system consisted of collaborative robot KUKA LBR iiwa 14 R820 with controller ("KUKA Systems GmbH," Germany), custom-designed extrusion 3D bioprinting device (3D Bioprinting Solutions, Russia), and software SprutCAM ("SPRUT Technology," Russia). Three-layer collagen meshes with living cells and PL were created according to the 3D CAM. The experimental setup also included the sensors for detecting respiratory movements and correcting the bioprinting path.

The printed patches (meshes with 0.6 mm pores) for skin wounds were produced following pre-calculated 3D models. The robotic-assisted system spent several minutes to determine the pattern of movement and to perform bioprinting. The sensors with feedback allowed bioprinting of complex structures without significant deviations from the digital model and damages to the subcutaneous tissues due to animals' breathing movements.

The *in vivo* experiments also demonstrated evident biocompatibility and healing potencies of complex bioinks. In all animals, the defects healed within 4 weeks – that is, wound contraction, matured re-epithelialization, and restoration of the hairs could be observed without any signs of inflammation or rejection (Figure 5E-H). Thus, the complex composition of bioinks allowed for complex 3D bioprinting without affecting its viscosity and polymerization and provided an excellent wound healing effect.

3.4. Fidelity

To assess the print quality, a test grid was printed. The resulting structure was photographed using a Nikon SMZ18 binocular microscope (Nikon, Japan). An image of the intended trajectory was superimposed on the resulting photo (Figure 6A). Then, the number of pixels that is outside the expected trajectory was calculated. Fidelity was calculated as the ratio of the error to the entire area of the trajectory. For the developed system, the fidelity was 93%.

3.5. Collagen contraction

We studied the contraction of collagen and collagen + platelet lysate gels by HF cells. As shown in Figure 7, the addition of platelet lysate increased the contraction of collagen gels. To quantitate gel contraction, the images of gels were obtained at 48 h, and the area of the gel was calculated and expressed as a percentage of the original area.

To assess the effect of platelet lysate on the spreading of HUVEC and HUVEC + HF spheroids, a 3D migration assay in a collagen and collagen + platelet lysate gels was performed. As shown in Figures 8A and 9A-C,E, the addition of platelet lysate dramatically improved the migration of HUVEC spheroids and changed the spreading pattern of HUVEC + HF spheroids.

For HUVEC spheroids, the spreading area increased by 2.3 times in collagen + platelet lysate gel and only by 1.2 times in collagen gel (Figure 8B). Despite the fact that the total area of spreading of HUVEC + HF spheroids in the two types of gels was comparable, the density of migrated cells was higher in the collagen + platelet lysate gel (Figure 9D).

3.6. Adhesiometric analysis

The level of adhesion of bioprinter hydrogel to non-injured and injured cadaveric human skin has been estimated using commercial adhesion tester and high level of adhesion has been demonstrated. The level of estimated adhesion of bioprinted hydrogel to injured rat cadaveric skin was higher (Figure 4C). There were also no statistically significant differences in the level of adhesion between the two types of hydrogel used in this study as bioinks.

3.7. The composition of bioink determines the intensity and complexity of regeneration processes

After applying the tissue-engineered composition to the area of the skin defect using a collaborative bioprinter, the wound was closed with a surgical dressing and left under dynamic observation for 4 weeks. At the end of this period, the animals were sacrificed, and after that, histological preparations were prepared for subsequent microscopic analysis. In the experiment, two types of bioink were used,

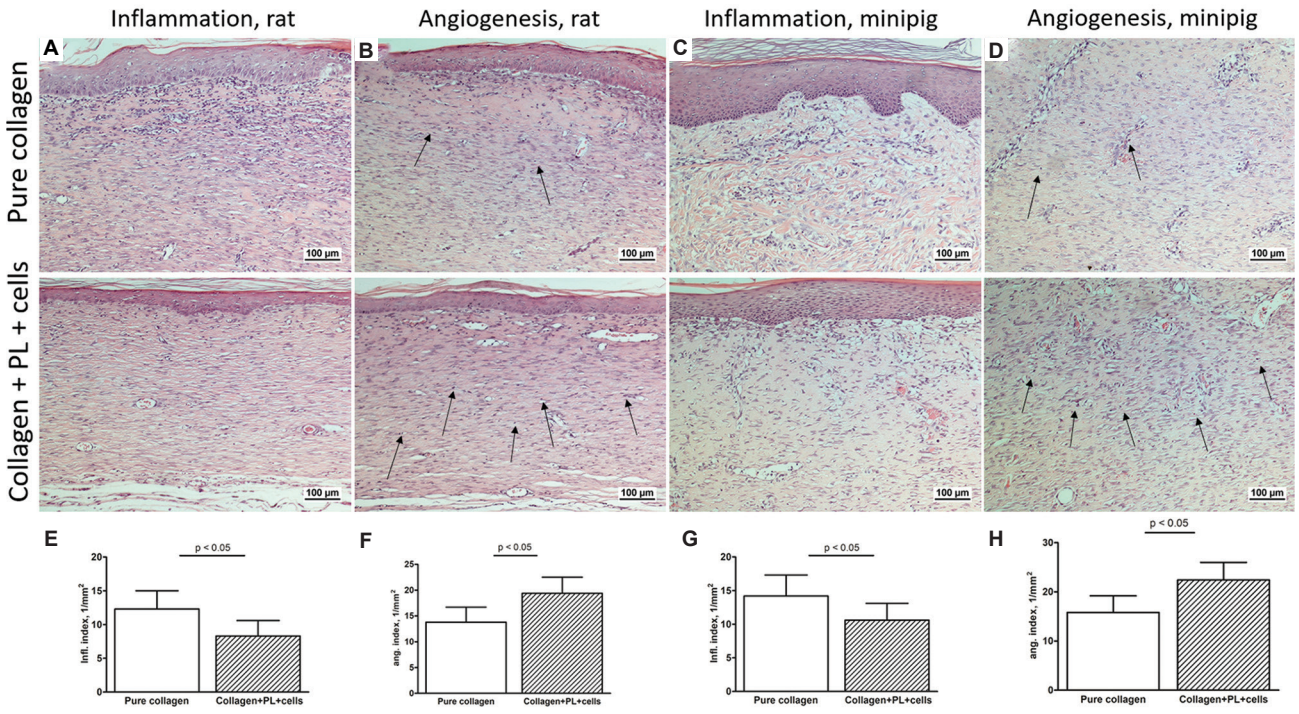

Figure 5. Histology morphometric analysis: (A) inflammatory histology in rat; (B) angiogenesis histology in rat; (C) inflammatory histology in minipig; (D) angiogenesis histology in minipig; (E) inflammatory index in rat; (F) angiogenesis index in rat; (G) inflammatory index in minipig; and (H) angiogenesis index in minipig.

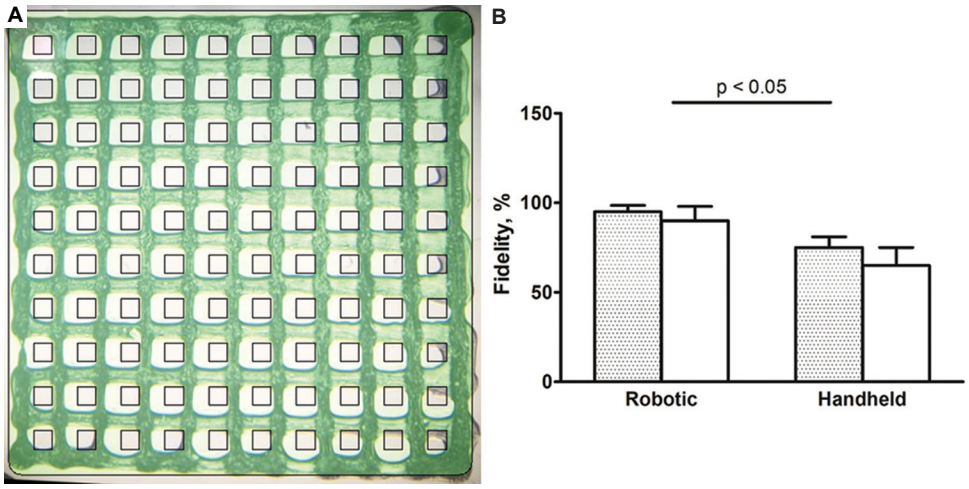

Figure 6. (A) Printed construct with CAD model and (B) comparison of bioprinting fidelity between *in situ* robotic printer and *in situ* handheld printer (shaded – *in vitro* bioprinting, white – *in vivo* bioprinting).

based on porcine collagen hydrogel brand "Viscoll" with high adhesiveness and viscosity. Pure collagen hydrogel was used as a control for *in situ* bioprinting, while composite bioinks was added with platelet lysate[33]. Cultured skin fibroblasts obtained from rats or pigs, respectively, were used in the experimental group. It should be noted that the bioprinting with both compounds of the hydrogel was not accompanied by the development of infectious processes or fibrous degeneration, indicating that the chosen collagen hydrogel had high rates of sterility and biocompatibility.

At the same time, a histological analysis performed 4 weeks after the surgical formation of a full-layer skin defect showed more advanced stages of regeneration in the case of using composite bioinks for *in situ* bioprinting. Apparently, the presence of a composition of soluble growth factors and

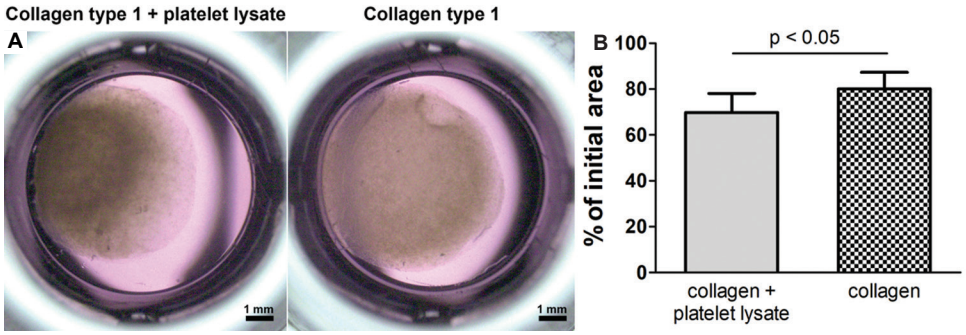

Figure 7. Contraction of collagen + platelet lysate and collagen gels by primary human fibroblasts. (A) Phase-contrast images and (B) reduction of the initial gel area after 48 h. Data represent mean ± SD, n = 8 samples per one data point. The differences between two groups are significant ($P < 0.05$, Mann–Whitney U-test).

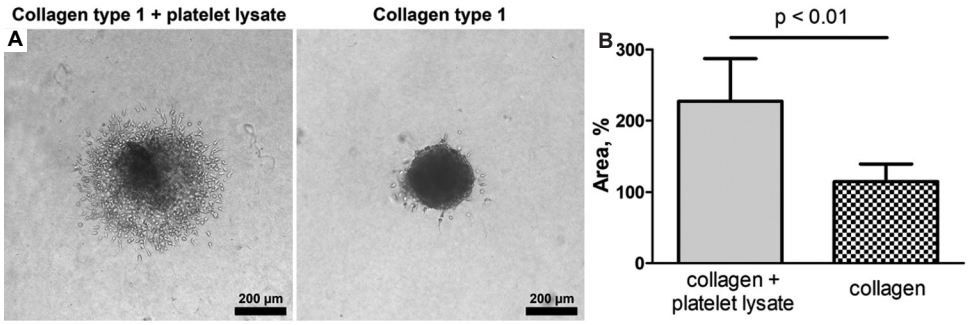

Figure 8. Spreading of HUVEC spheroids in collagen + platelet lysate and collagen gels. (A) Phase-contrast images and (B) expansion of the spreading area after 48 h. Data represent mean ± SD, n = 8 spheroids per one data point. The differences between two groups are significant ($P < 0.01$, Mann–Whitney *U*-test).

cytokines (mainly PDGF, VEGF, IGF, etc.) in platelet lysate released during preparation, as well as trophic and reparative effects of living fibroblasts, accelerated the healing process. Thus, after 4 weeks, defects covered with pure collagen still showed signs of an early inflammatory (exudative) phase of regeneration, which was accompanied by the presence of a large number of polymorphonuclear leukocytes and monocytes in the subepidermal regions and derma (Figure 5A and C). At the same time, the use of composite bioinks shifted the regeneration process toward the completion of the proliferative phase with the predominance of active remodeling processes. In both animal models, the addition of platelet lysate and fibroblasts to the bioink composition significantly stimulated angiogenesis processes and formation of a more mature skin (Figure 5B and D). Thus, the introduction of biologically active factors into the composition of the collagen hydrogel, on the one hand, did not affect the rheological properties of the bioink that was critical for the bioprinting procedure, and on the other hand, made it possible to enhance the regenerative properties of the developed approach. However, the conducted research did not allow us to confirm the direct incorporation of the introduced fibroblasts into the structure of the newly formed dermis. This issue is planned to be studied in our ongoing studies.

4. Discussion

The most important result of present investigation was the design and fabrication of the world's first commercial articulated collaborative *in situ* bioprinter**.** We used commercially available articulated (with 6 degrees of freedom) collaborative robotic hand originally developed by German company Kuka**.** Kuka robotic hand has a high level of printing resolution (or repetition) and it well protects users, such as surgeons and patients in our case (built in collaborative capacities), from potential undesirable injury. Moreover, Kuka's collaborative robotic hand employed in our *in situ* bioprinter has been already certified for clinical use. However, the nozzle or head of bioprinter was our original design, and the correspondent software for printing on moving and curve surfaces was originally developed. The *in situ* bioprinter demonstrated high printing resolution and fidelity (Figure 6B) both *in vitro* on static dried plastic surface and *in vivo* on wet curvy wound surface during animal breathing and moving (Figure 10). The employed original composition of collagen hydrogel-based bioink has shown strong attachment and even adhesion of printed bioink to the wet wound surface. Removal of bioprinted bioinks strongly attached to the

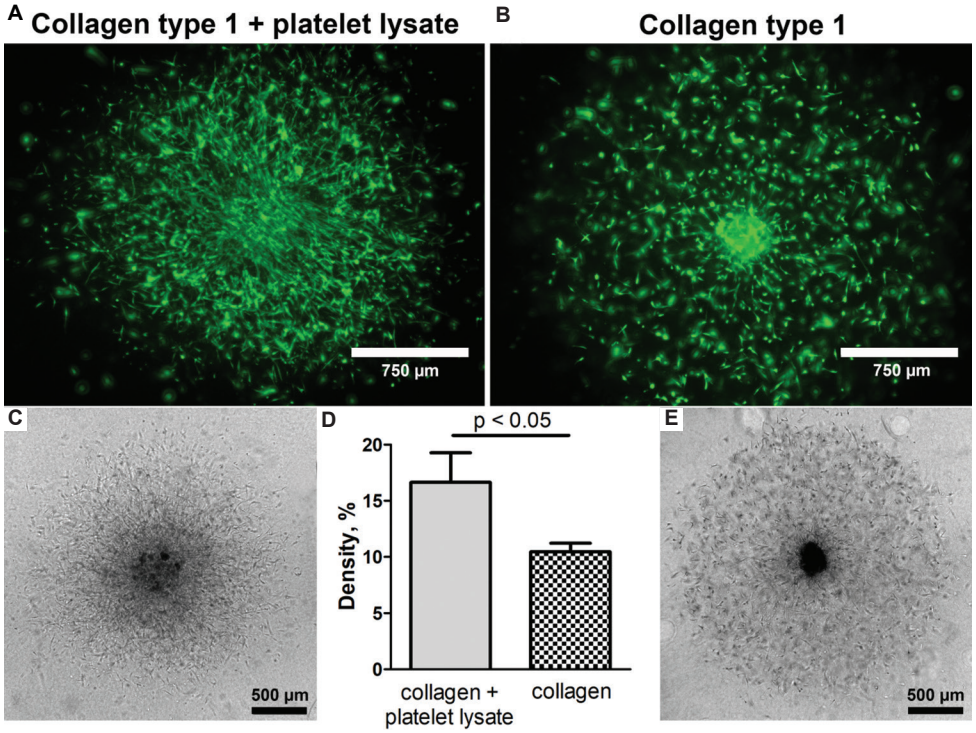

Figure 9. Spreading of HUVEC + HF spheroids in collagen + platelet lysate and collagen gels. (A, B) Fluorescent images; (C, E) phase-contrast images; and (D) cell density after 48 h. Data represent mean ± SD, $n = 8$ spheroids per one data point. The differences between two groups are significant ($P < 0.05$, Mann–Whitney U-test).

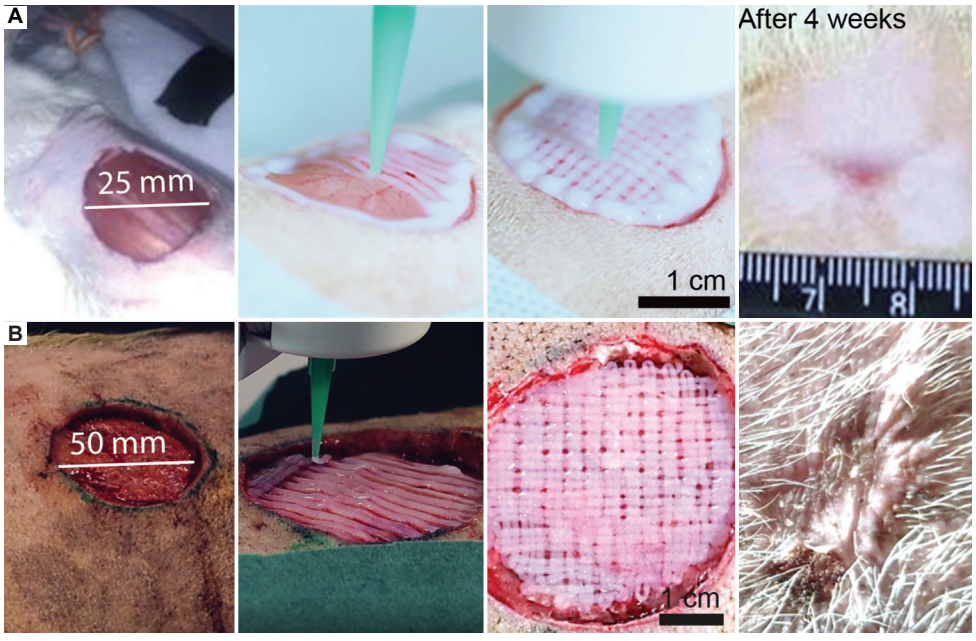

Figure 10. *In vivo* bioprinting in animal experiments: (A) Rats and (B) minipigs. High levels of bioprinting fidelity have been demonstrated both in rats and in minipigs.

wound surface was no trivial task and required special efforts. *In situ* bioprinter is relatively easy to operate and monitor. The special originally developed software enables bioprinting processes both on curvy and moving wound surfaces. The fact that we used commercially available articulated collaborative robotic hand already certified for

clinical use as an integral basic part of our original *in situ* bioprinter will enable its serial standard production as well as regulatory approval and certification for clinical use and desirable commercialization. With growing market penetration and scaling as well as automated serial manufacturing, the cost for developing *in situ* bioprinter will be significantly reduced, thereby making the bioprinter both affordable and clinically relevant.

To estimate the feasibility of *in situ* bioprinting technology using original articulated *in situ* bioprinter, we tested it on experimental animal models of wound closure. It have been demonstrated that *in situ* bioprinter enabled *in situ* bioprinting of original bioink with high level of fidelity and adhesion on the wet curved wound's surfaces of breathing animals. Moreover, the dynamic observation of skin wound healing in control and experimental groups both in rats and minipigs revealed the strong enhancing effect of *in situ* bioprinting of original bioink on the dynamics of wound healing process: (i) Although wound closure was practically the same in both groups, the wound contraction was accelerated; (ii) level of vascularization was increased; (iii) the inflammation was reduced and was more modest; and finally, (iv) the manifestation of fibrosis during wound healing was significantly reduced. Taken together, these observations demonstrate the positive effect of *in situ* bioprinting on the dynamics and quality of skin wound healing process which is in very good agreement with earlier published reports[34].

To understand possible mechanisms of enhancing effect of *in situ* bioprinting on skin would healing, two additional *in vitro* experiments were performed. In the first experiment, we used classic collagen contraction assay[35], but instead of conventional simple collagen hydrogel, we used bioink containing collagen hydrogel, 5% platelet lysate, and human dermal fibroblasts. It was demonstrated that addition of platelet lysate to collagen hydrogel increasing level of collagen hydrogel contraction by human dermal fibroblasts. In the second *in vitro* experiment, it was demonstrated the significant increase of *in vitro* sprouting angiogenesis from tissue spheroids embedded in 3D collagen hydrogel from original bioink with addition of 5% platelet lysate containing a lot of angiogenic growth factors as compared with pure collagen hydrogel "Viscoll." These data at least partly explain the enhanced wound healing effect *in vivo*. Thus, it is logical to speculate that enhancement of wound contraction in our *in vivo* experiments could be explained by *in situ* bioprinted hydrogel contraction induced by dermal fibroblasts.

The possible mechanisms of enhanced skin wound healing by employing *in situ* bioprinting technology are summarized in the scheme presented in Figure 11. The advantages of *in situ* bioprinting technology are presented in Figure 12.

In the end, we would like to summarize the main advantages of new *in situ* bioprinter as compared with standard *in vitro* 3D bioprinter and with cost-effective *in situ* handheld bioprinter (Table 1). *In situ* bioprinting technology has obvious imitations and it is useful mainly for the treatment of skin defects and some endoscopic applications. Theoretically, such robotic system could be useful for bioprinting in the area of extended defects with prominent curvature. Thus, the best results can be achieved in the treatment of skin defects in the axillary or interscapular regions, as well as while covering lesions of the oral mucosa or cornea. The main advantage of *in situ* bioprinting is that it does not need extremely expensive and labor-consuming GMP facilities as well as additional bioreactors, because the organism itself performs this function.

Despite the fact that handheld devices can in some cases replace a complex and massive robotic system for *in situ* bioprinting, especially in hard-to-reach localizations (for example, articular cartilage or the terminal gastrointestinal tract mucosa), low precision, and printing resolution significantly limit their therapeutic capabilities.

The main task of classical *in vitro* bioprinting, in our opinion, is creating complex tubular and solid organs, which require a combination of different types of cells and biomaterials with the reconstruction of the complex internal structure of the parenchyma, blood vessels, and nerves. Such tissue engineering products must undergo a long cycle of post-processing maturation in a perfusion bioreactor before they can be transplanted into the patient's body.

Theoretically, it is difficult to expect an enhancement of normal regenerative processes during skin wound healing because wound healing is a very robust process. Moreover, it has been indeed demonstrated in this study as well as in previously published publication[34] that *in situ* bioprinting technology at least did not dramatically change or interfere with the normal dynamics of wound healing processes (Supplementary File). Taken together, however, our *in vivo* and *in vitro* data strongly suggest a potentially strong enhancement of human skin wound healing using *in situ* bioprinting in specific cases of skin pathological conditions. Thus, it is logical to speculate that *in situ* bioprinting technology could be potentially useful as a novel therapeutic modality for more effective treatment and enhancement of wound healing processes in different types of skin pathologies, such as burns, diabetic foot ulcer, or certain genetic skin diseases (especially, for example, epidermolysis bullosa).

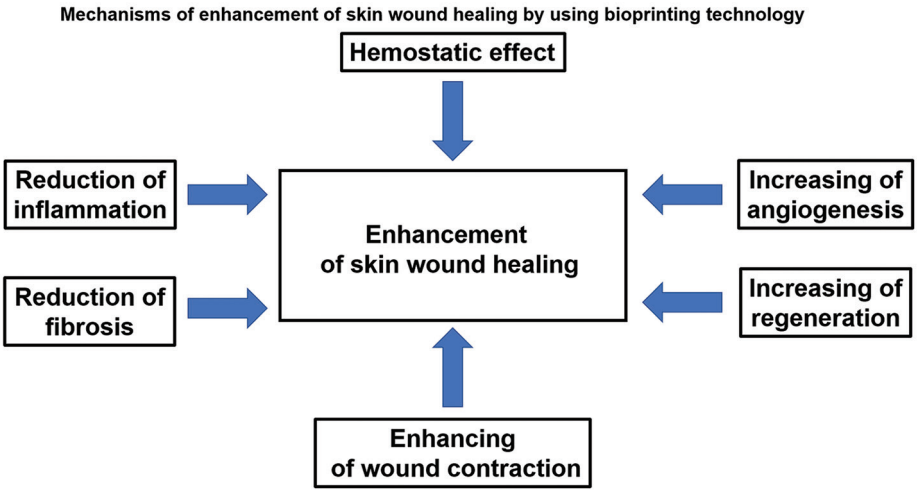

Figure 11. Possible mechanisms of enhancement of human skin wound healing using *in situ* bioprinting technology.

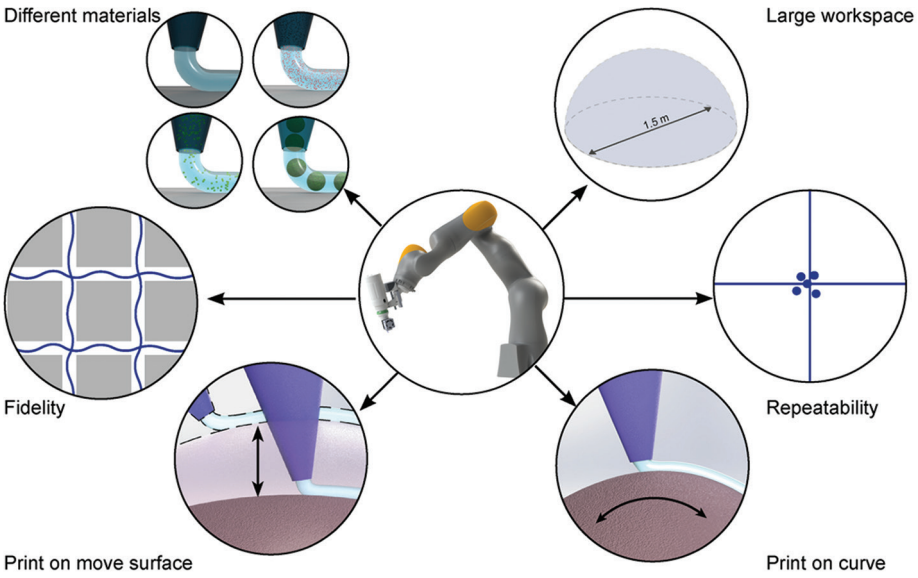

Figure 12. The main advantages of *in situ* bioprinting technology.

Table 1. Comparative analysis of advantages and disadvantages of different variants of bioprinting technologies

Type of bioprinter	GMP	Surgery	Repeatability	Cost	Bioreactor
In situ bioprinter	–	+	↑	↑	-
In vitro bioprinter	+	–	↑	↑	+
Handheld printer	–	+	↓	↓	-

5. Conclusion

Development, implementation, and initial *in vitro* and *in vivo* experimental testing of the world's first commercial *in situ* bioprinter are reported and described in this paper. It has been demonstrated that articulated *in situ* bioprinter has safe collaborative robotic arm, unique capacity for bioprinting on wet surfaces of complex geometry and curvature with strong adhesion, and high level of printing fidelity. The *in vivo* experiments demonstrated that the employed original bioinks based on collagen hydrogel, platelet lysate, and dermal fibroblasts significantly improve the quality of wound healing processes in rat and minipig skin wounds. Increased contraction in *in vitro* collagen contraction assay as well as promoting of *in vitro* sprouting angiogenesis from tissue spheroids embedded in 3D collagen hydrogel from original bioink at least partly explain the enhancement of wound healing effect *in vivo*. Thus, *in situ* bioprinting is a very promising

perspective variant of 3D bioprinting technology and the further development and successful clinical applications of commercial *in situ* bioprinters are highly desirable[36].

Acknowledgments

None.

Funding

This work was funded by the Ministry of Science and Higher Education of the Russian Federation under the strategic academic leadership program "Priority 2030."

Conflict of interest

The authors declare no conflicts of interest.

Author contributions

Conceptualization: Vladimir A. Mironov and Vadim L. Zorin

Formal analysis: Sergey P. Domogatsky and Vladislav A. Parfenov

Funding acquisition: Yusef D. Khesuani

Investigation: Pavel A. Karalkin, Elizaveta V. Koudan, and Egor O. Osidak

Methodology: Alexey V. Kovalev and Vladimir A. Kasyanov

Resources: Fedor S. Senatov

Software: Aleksandr A. Levin

Visualization: Frederico D.A.S. Pereira

Writing – original draft: Vladislav A. Lvov and Stanislav V. Petrov

Writing – review and editing: Natalya E. Manturova and Natalia S. Sergeeva

Ethics approval and consent to participate

Experiments on animals have been approved Ethical Committee of The National Medical Research Radiological Center, P. A. Hertsen Moscow Oncology Research Center, Moscow, Russia, by the local ethics committee (protocol #0120/19 dated November 1, 2019).

Consent for publication

Not applicable.

Availability of data

Not applicable.

References

1. Murphy SV, Atala A, 2014, 3D bioprinting of tissues and organs. *Nat Biotechnol*, 32: 773–785.

   https://doi.org/10.1038/nbt.2958

2. Sun W, Starly B, Daly AC, *et al.*, 2020, The bioprinting roadmap. *Biofabrication*, 12: 022002.

   https://doi.org/10.1088/1758-5090/ab5158

3. Murphy SV, De Coppi P, Atala A, 2020, Opportunities and challenges of translational 3D bioprinting. *Nat Biomed Eng*, 4: 370–380.

   https://doi.org/10.1038/s41551-019-0471-7

4. Ozbolat IT, 2015, Bioprinting scale-up tissue and organ constructs for transplantation. *Trends Biotechnol*, 33: 395–400.

   https://doi.org/10.1016/j.tibtech.2015.04.005

5. Mironov V, Kasyanov V, Drake C, *et al.*, 2008, Organ printing: Promises and challenges. *Regen Med*, 3: 93–103.

   https://doi.org/10.2217/17460751.3.1.93

6. He J, Mao M, Li X, *et al.*, 2021, Bioprinting of 3D functional tissue constructs. *Int J Bioprint,* 7: 395.

   https://doi.org/10.18063/ijb.v7i3.395

7. Mironov V, Boland T, Trusk T, *et al.*, 2003, Organ printing: Computer-aided jet-based 3D tissue engineering. *Trends Biotechnol*, 1: 157–161.

   https://doi.org/10.1016/S0167-7799(03)00033-7

8. Zhang J, Wehrle E, Rubert M, *et al.*, 2021, 3D bioprinting of human tissues: Biofabrication, bioinks, and bioreactors. *Int J Mol Sci*, 22: 3971.

   https://doi.org/10.3390/ijms22083971

9. Yeong WY, Chua CK, Leong KF, *et al.*, 2004, Rapid prototyping in tissue engineering: Challenges and potential. *Trends Biotechnol*, 22: 643–652.

   https://doi.org/10.1016/j.tibtech.2004.10.004

10. Ng WL, Chua CK, Shen YF, 2019, Print me an organ! Why we are not there yet. *Prog Polym Sci*, 97: 101145.

    https://doi.org/10.1016/j.progpolymsci.2019.101145

11. Weng T, Zhang W, Xia Y, *et al.*, 2021, 3D bioprinting for skin tissue engineering: Current status and perspectives. *J Tissue Eng*, 12: 20417314211028574.

    https://doi.org/10.1177/20417314211028574

12. Gao C, Lu C, Jian Z, *et al.*, 2021, 3D bioprinting for fabricating artificial skin tissue. *Colloids Surf B Biointerfaces,* 208: 112041.

    https://doi.org/10.1016/j.colsurfb.2021.112041

13. Martin I, Wendt D, Heberer M, 2004, The role of bioreactors in tissue engineering. *Trends Biotechnol*, 22: 80–6.

    https://doi.org/10.1016/j.tibtech.2003.12.001

14. Hansmann J, Groeber F, Kahlig A, et al., 2013, Bioreactors in tissue engineering-principles, applications and commercial constraints. *Biotechnol J*, 8: 298–307.

    https://doi.org/10.1002/biot.201200162

15. Martin I, Smith T, Wendt D, 2009, Bioreactor-based roadmap for the translation of tissue engineering strategies into clinical products. *Trends Biotechnol*, 27: 495–502.

https://doi.org/10.1016/j.tibtech.2009.06.002

16. Singh S, Choudhury D, Yu F, *et al*., 2019, *In situ* bioprinting-bioprinting from benchside to bedside? *Acta Biomater*, 101: 14–25.

https://doi.org/10.1016/j.actbio.2019.08.045

17. Samandari M, Mostafavi A, Quint J, *et al*., 2022, *In situ* bioprinting: Intraoperative implementation of regenerative medicine. *Trends Biotechnol*, 40: 1229–1247.

https://doi.org/10.1016/j.tibtech.2022.03.009

18. Dias JR, Ribeiro N, Baptista-Silva S, *et al*., 2020, *In situ* enabling approaches for tissue regeneration: Current challenges and new developments. *Front Bioeng Biotechnol*, 8: 85.

https://doi.org/10.3389/fbioe.2020.00085

19. Ashammakhi N, Ahadian S, Pountos I, *et al*., 2019, *In situ* three-dimensional printing for reparative and regenerative therapy. *Biomed Microdevices*, 21: 42.

https://doi.org/10.1007/s10544-019-0372-2

20. Wu Y, Ravnic DJ, Ozbolat IT, 2020, Intraoperative bioprinting: repairing tissues and organs in a surgical setting. *Trends Biotechnol*, 38: 594–605.

https://doi.org/10.1016/j.tibtech.2020.01.004

21. Neng X, Guohong S, Yuling S, *et al*., 2020, Research progress of robot technology in *in situ* 3D bioprinting. *Int J Bioprint*, 8: 614.

https://doi.org/10.18063/ijb.v8i4.614

22. Choudhury D, Anand S, Naing MW, 2018, The arrival of commercial bioprinters-towards 3D bioprinting revolution! *Int J Bioprint*, 4: 139.

https://doi.org/10.18063/IJB.v4i2.139

23. Wang M, He J, Liu Y, *et al*., 2015, The trend towards *in vivo* bioprinting. *Int J Bioprint*, 1: 15–26.

https://doi.org/10.18063/IJB.2015.01.001

24. Ding H, Chang RC, 2018, Simulating image-guided *in situ* bioprinting of a skin graft onto a phantom burn wound bed. *Addit Manuf*, 22: 708–719.

https://doi.org/10.1016/j.addma.2018.06.022

25. Fortunato GM, Rossi G, Bonatti AF, *et al*., 2021, Robotic platform and path planning algorithm for in situ bioprinting. *Bioprinting*, 22: e00139.

https://doi.org/10.1016/j.bprint.2021.e00139

26. Di Bella C, Duchi S, O'Connell CD, *et al*., 2018, *In situ* handheld three-dimensional bioprinting for cartilage regeneration. *J Tissue Eng Regen Med*, 12: 611–621.

https://doi.org/10.1002/term.2476

27. Hakimi N, Cheng R, Leng L, *et al*., 2018, Handheld skin printer: *In situ* formation of planar biomaterials and tissues. *Lab Chip*, 18: 1440–1451.

https://doi.org/10.1039/c7lc01236e

28. Albanna M, Binder KW, Murphy SV, *et al*., 2019, *In situ* bioprinting of autologous skin cells accelerates wound healing of extensive excisional full-thickness wounds. *Sci Rep*, 9: 1856.

https://doi.org/10.1038/s41598-018-38366-w

29. Pazhouhnia Z, Beheshtizadeh N, Namini MS, *et al*., 2022, Portable hand-held bioprinters promote *in situ* tissue regeneration. *Bioeng Transl Med*, 7: e10307.

https://doi.org/10.1002/btm2.10307

30. Campos DF, Zhang S, Kreimendahl F, *et al*., 2020, Hand-held bioprinting for de novo vascular formation applicable to dental pulp regeneration. *Connect Tissue Res*, 61: 205–215.

https://doi.org/10.1080/03008207.2019.1640217

31. Osidak EO, Karalkin PA, Osidak MS, *et al*., 2019, Viscoll collagen solution as a novel bioink for direct 3D bioprinting. *J Mater Sci Mater Med*, 30: 31.

https://doi.org/10.1007/s10856-019-6233-y

32. Shansky YD, Sergeeva NS, Sviridova IK, *et al*., 2019, Human platelet lysate sustains the osteogenic/adipogenic differentiation potential of adipose-derived mesenchymal stromal cells and maintains their dna integrity *in vitro*. *Cells Tissues Organs*, 207: 149–164.

https://doi.org/10.1159/000502813

33. Lang S, Loibl M, Herrmann M, 2018, Platelet-rich plasma in tissue engineering: Hype and hope. *Eur Surg Res*, 59: 265–275.

https://doi.org/10.1159/000492415

34. Nuutila K, Samandari M, Endo Y, *et al*., 2022, *In vivo* printing of growth factor-eluting adhesive scaffolds improves wound healing. *Bioact Mater*, 8: 296–308.

https://doi.org/10.1016/j.bioactmat.2021.06.030

35. Montesano R, Orci L, 1988, Transforming growth factor beta stimulates collagen-matrix contraction by fibroblasts: Implications for wound healing. *Proc Natl Acad Sci U S A*, 85(13):4894-7.

https://doi.org/10.1073/pnas.85.13.4894

36. Popp CM, Miller WC, Eide CR, *et al*., 2022, Future applications of 3D bioprinting: A promising technology for treating recessive dystrophic epidermolysis bullosa. *Exp Dermatol*, 31: 384–392.

https://doi.org/10.1111/exd.14484